A PRECISION ANGULAR CORRELATION TABLE

AND CALCULATION OF GEOMETRICAL CORRECTION FACTORS

APPROVED:

Tom J. Gray
Major Professor

H. D. Mackey
Minor Professor

J. Sybert
Director of the Department of Physics

Robert B. Toulouse
Dean of the Graduate School

# A PRECISION ANGULAR CORRELATION TABLE AND CALCULATION OF GEOMETRICAL CORRECTION FACTORS

THESIS

Presented to the Graduate Council of the
North Texas State University in Partial
Fulfillment of the Requirements

For the Degree of

MASTER OF SCIENCE

By

Larry James Rowton, B. S.
Denton, Texas
January, 1970

TABLE OF CONTENTS

LIST OF TABLES

LIST OF ILLUSTRATIONS

# CHAPTER I

## INTRODUCTION

In 1940[1] Hamilton reported the results of the theoretical investigations of the directional correlations between sequentially emitted radiations from excited nuclei. Further theoretical work[2-6] has refined the original treatment and extended it to include extranuclear effects.

In recent years $\gamma$-$\gamma$ angular correlations have been very useful in confirming the spins of excited nuclear states. Angular correlation techniques have also been employed to study the electric and magnetic character of excited nuclear states. With these things in mind, it was decided to design, construct, and test a precision angular correlation table. Most experimenters of the past have used NaI detectors for the detection of the $\gamma$-radiations. NaI detectors have good detection efficiencies but relatively poor energy resolutions. On the other hand, the newer Ge(Li) detectors have poorer efficiencies because of the small active volumes of such detectors. However, Ge(Li) detectors have much better energy resolutions by approximately a factor of ten to thirty. The work of this correlation laboratory at N.T.S.U. is planned around investigating the rare earth nuclei, which have very

complex γ-ray energy spectra. Hence, it is necessary to use the higher resolution Ge(Li) detectors on the correlation table in order to resolve the spectrum components of interest.

It was decided to use the directional correlation of $^{106}Pd$ to calibrate the table. $^{106}Pd$ was chosen because its correlation is well structured and has been measured by several observers.[9-12] Figure 1 shows the decay scheme of $^{106}Pd$. The correlation of interest is the 624-513 KeV γ-γ cascade. The 624-513 KeV transitions are E2-E2 in character.

The photons emitted by an unoriented sample in which a large number of nuclei are undergoing identical γ-ray transitions will be isotropic in laboratory coordinates. There is no preferred direction of emission for the γ-ray photon from the individual transition $I_A \xrightarrow{\gamma} I_B$ because the decaying nuclei are randomly oriented. If the transition $I_A \xrightarrow{\gamma} I_B$ is followed by a second transition $I_B \xrightarrow{\gamma} I_C$, the individual radiations from the second transition are likewise isotropic in the laboratory coordinates. However, in a two-step cascade, such as $I_A \xrightarrow{\gamma} I_B \xrightarrow{\gamma} I_{B,C}$, there is an angular correlation between the directions of emission of two successive γ-ray photons, $\gamma_1$ and $\gamma_2$, which are emitted from the same nucleus.

Evans[13] gives a simple pictorial development of angular correlations between successive γ-rays. In the following discussion his development will be followed.

The existence of an angular correlation arises because the direction of the first radiation is related to the

orientation of the angular momentum $I_B$ of the intermediate level. This orientation can be expressed in terms of the magnetic-angular-momentum quantum number $m_B$ with respect to some laboratory direction such as that of the first $\gamma$-ray. If $I_B$ is not zero, and if the lifetime of the intermediate level is short enough so that $I_B$'s orientation persists, then the direction of the second $\gamma$-ray will be related to the direction of $I_B$ and therefore to the direction of the first $\gamma$-ray.

Let a $\gamma$-$\gamma$ cascade be represented by the notation $I_A(j_1)I_B(j_2)1_C$, where $j_1$ and $j_2$ are the angular momenta of the two successive $\gamma$-rays. The simplest case to discuss is two successive dipole $\gamma$-rays ($j_1=j_2=1$) in the cascade $0(1)1(1)0$.

At first, imagine that measurements are made only on the second $\gamma$-ray, and that the source is in a magnetic field H, which serves here to give a fixed direction in the laboratory. The magnetic sublevels $m_B=0,\pm1$ of the excited level $I_B$ are shown schematically in Figure 2. The magnetic sublevels are equally populated under ordinary experimental conditions, and therefore the transitions $m = 0, \pm 1$, will have equal probabilities.

The angular distribution of the intensity of electric multipole radiation is given by known analytic functions and is the same for electric $2^j$-pole and magnetic $2^j$-pole radiation. For dipole radiation, the angular distribution is

$$W^{0}(\theta)\, d\Omega = \frac{3}{8\pi} \sin^{2}\theta d\Omega \text{ for } m = 0 \qquad (1.1)$$

$$W^{+1}(\theta)\, d\Omega = \frac{3}{16\pi} (1+\cos^{2}\theta)\, d\Omega \text{ for } m = +1 \qquad (1.2)$$

$$W^{-1}(\theta)\, d\Omega = \frac{3}{16\pi} (1+\cos^{2}\theta)\, d\Omega \text{ for } m = -1, \qquad (1.3)$$

where $\theta$ is the angle between H and the direction of emission of the photon, and $W(\theta)$ is the probability per unit solid angle that the photon is emitted into the solid angle $d\Omega$ at $\theta$.

If the states are equally populated, the total angular distribution is the sum of equations 1.1, 1.2, and 1.3, which is a constant. Even in the presence of the ordinary magnetic field, the total radiation is still isotropic. The observation of an isotropy in the angular distribution depends on the ability to obtain a nonuniform population of magnetic substates. This can be done most simply for the dipole case if it can be arranged experimentally to exclude observation of the $m = 0$ transitions. The angular distribution of the $m = \pm 1$ transitions would then have a $(1+\cos^{2}\theta)$ distribution.

Experimentally this can be done by forming the $m_B=0$ sublevel in a preceding transition $I_A \xrightarrow{\gamma} I_B$ as shown in Figure 3. No magnetic field is used. In its absence, the $m_B$ sublevels are degenerate, and the transition probabilities from $I_A=0$, $m_A=0$ to each of the $m_B$ sublevels are equal. Since now the direction of $\theta=0$ in the laboratory is arbitrary, it can be chosen as the direction of emission of the first $\gamma$-ray, $\gamma_1$. The first transition cannot lead to the sublevel $m_B=0$ in this particular coordinate system, because by equation 1.1 its

intensity in the $\theta=0$ direction is zero. Therefore, all of the $\gamma$ -rays in the $\theta=0$ direction correspond to $m_1=\pm 1$ transitions. The $m_1=+1$ transition has to be followed by $m_2=-1$, and likewise for $m_1=-1$ and $m_2=+1$, in order to reach $I_C=0$ as required by the conservation of angular momentum. Both of these second transitions have a $(1+\cos^2\theta)$ distribution. Thus, if $\gamma_1$ is detected in a counter whose direction from the source is called $\theta=0$, the probability that $\gamma_2$ will impinge on a second detector set at an angle $\theta$ will vary as $(1+\cos^2\theta)$.

This discussion is applicable only to the 0(1)1(1)0 cascade, of which there is no known nuclear example. However, the principles which have just been outlined can be applied to any $\gamma$-$\gamma$ cascade involving arbitrary multipole orders, but mathematical complications rapidly become insuperable unless more advanced methods are used. For the generalized cascade $I_A(j_1)I_B(j_2)I_C$ the angular correlation function $W(\theta)$ for the angle $\theta$ between the successive $\gamma$-rays can be shown to be[3,7,8]

$$W(\theta)d\Omega = \sum_{i=0}^{i=L} A_{2i}P_{2i}(\cos\theta)d\Omega, \qquad (1.4)$$

where $A_{2i}$ are coefficients which depend on $j_1$ and $j_2$, and $P_{2i}(\cos\theta)$ are the even Legendre polynomials. The coefficients $A_{2i}$ can be calculated from tables given by Rose.[6]

Klema and McGowan[7] performed the 624-513 KeV correlation in $^{106}$Pd in 1953. Their experiment was based upon the use of two 1.5-inch by 1-inch NaI detectors as $\gamma$-ray spectrometers. They used the results of Rose[10] to correct for the finite

solid angles of their detectors. The values, corrected for finite geometries, which they reported are

$$A_2 = 0.3456 \pm 0.0079 \text{ and } A_4 = 1.109 \pm 0.012.$$

Ortabasi and Körner[8] studied the $^{106}$Pd correlation in 1965. They report values for the correlation coefficient:

$$A_2 = 0.314 \text{ and } A_4 = 1.058.$$

No error bars for $A_2$ and $A_4$ were given in their paper. The latest published correlation of $^{106}$Pd was reported by J. Koch *et al.*[9] Their results for the determination of the correlation coefficients were

$$A_2 = 0.332 \pm .005 \text{ and } A_4 = 1.060 \pm 0.008.$$

# CHAPTER II

## APPARATUS AND DATA

The precision angular correlation table consists basically of two four-cubic-centimeter planar Ge(Li) detectors, mounted such that the axes of the two detectors lie in a horizontal plane and so that the detectors are rotatable about a central vertical axis. The radioactive source under observation is placed on this central axis in the plane of the detectors. The table is constructed so that the angle between the two detectors can be measured very accurately by use of a travel-dial indicator.

An isometric drawing of the table is given in Figure 4. The main support member of the table is a surface-ground cast-steel plate approximately 118.7 by 91.4 by 1.9 cm. Mounted on the baseplate is a track in the shape of a decagon constructed from ten cold roll steel plates approximately 35.6 by 7.62 by 0.95 centimeters. Each plate is bolted to the baseplate by two ¼ inch-28 machine screws. Four 8-32 set screws are mounted in each plate for leveling purposes. Thus each section of the track can be optically aligned until the entire track is in a horizontal plane. The carts which support the Ge(Li) detectors roll on this track. The carts

are pivoted on a central axle which is attached perpendicularly to a 50.8 cm diameter horizontal steel plate. This disk is rigidly mounted to the baseplate by eight 2.54 cm diameter by 6.99 cm long stainless steel standoffs.

Along the axis of the axle for the carts a 2.54 cm hole is bored such that it is a tight slip fit for a 2.54 cm stainless steel shaft. The purpose of this shaft is to locate and support the source holder. The source holder consists of an 0.5-inch 13 adjustment screw which has a hole drilled and tapped for a 10-24 screw in its top. The source container could then be attached to the adjustment screw by a 10-24 screw.

The detector cryostats are clamped to their respective dewars and the dewars are clamped to the carts. A travel-dial indicator is mounted under each detector cart. The travel-dials' measuring wheels are in contact with the circumference of the 50.8 cm disk. The travel-dials are used to measure the angles through which the detectors are rotated. They do this by measuring the subtended arc length, and since the radius is accurately known, the angles are directly calculable. The travel-dials will measure down to .0025 cm; therefore, the smallest change in angle measureable is one part in ten thousand.

The carts are constructed so that the distance from the source to the detectors can be varied. This will allow the half angle subtended by the front face of the detector to be varied from approximately $2^{o}$ to $39^{o}$.

The correlation table was set up in the following manner. All leveling and aligning was done with two Brunson telescopic transits with optical micrometer attachments. Horizontal planes were established with the horizontal transit and vertical planes were established with the vertical transit. The baseplate was leveled by setting a scale on the highest corner and reading the scale with the transit. Then the scale was moved to each of the other three corners and readings taken at each corner. Leveling screws on each leg supporting the baseplate were adjusted until the readings at each corner indicated that the baseplate was as level as possible.

The next leveling problem was the decagon track. First an arbitrary plate was selected. This section of the track was leveled by placing a scale first on one end of the plate and then on the other end and reading the scale with the transit. The plate was adjusted until the same reading was obtained at both ends. Then the other nine plates were leveled to this plate in a similar manner. By use of this procedure the entire track was leveled in a horizontal plane to $\pm 0.01$ cm.

The central disk was leveled by a similar procedure into a plane parallel to the track. Adjustments were made by placing shims under the stainless steel standoffs.

The vertical 2.54 cm shaft was aligned perpendicular to the central disk. Shims were used for adjustment.

A $^{22}Na$ correlation was performed to determine the 180° position of the two detectors. $^{22}Na$ is an ideal source for this purpose because it decays by positron emission, which in turn annihilates giving off two 511 KeV $\gamma$-rays which are at 180° with respect to one another. Thus, with this source maximum coincidences should be obtained when the detectors are 180° from one another. A plot of the $^{22}Na$ correlation is given in Figure 5. The center of the plot gives the 180° position of the detectors with respect to the travel-dial's zero.

Figure 6 shows a block diagram of the electronics used in this experiment. The signals from the detectors go to preamplifiers, then to amplifiers, and then to timing single channel analyzers (TSCA). The negative output signal from the movable detector's TSCA is used as the start signal for the time-to-amplitude converter (TAC). The negative output from the fixed detector's TSCA goes to a nanosecond delay box and then is used as the stop signal for the TAC. The output signal from the TAC is fed into a 1024 channel multichannel analyzer. The nanosecond delay box is used to calibrate the horizontal axis of the multichannel analyzer. Figure 7 shows a typical time spectrum. This figure shows the resolving time to be twenty nanoseconds full-width-half-maximum. The flat portion of the spectrum is due to the accidental coincidences. The TAC spectrum thus gives the true and accidental counting rates simultaneously. The resolving time of the system is

approximately 1.5 nsec for signals derived from a pulser signal in both start and stop channels. For detector pulses, the resolving time of the coincidence spectrum varies from approximately 12 nsec to 20 nsec depending upon the window widths of the single channel analyzers. The system uses cross-over pickoff timing, and as a result the time resolution depends directly on the window widths of the single channel analyzers. The resolving time also depends on the location at which the $\gamma$-ray photon is absorbed by the detector because a finite amount of time is required to collect the charge produced by a $\gamma$-ray interacting with the detector material. Thus, different times are required to collect the charges produced by $\gamma$-rays that are absorbed in different volumes of the detector. Because of this volume effect, pulses will have a distribution of pulse rise times.

Originally, a plated $^{106}Ru$ source was to have been used in this experiment. When the source was purchased it was in the form of $RuCl_3$ dissolved in HCl. This solution was not useable as a plating electrolyte; therefore, the $RuCl_3$ was nitrated to ruthenium nitroso. Nitroso compounds are usually unstable and decompose in a few hours. The plate obtained was not uniform; hence, the $\gamma$-ray flux from this source was not isotropic, and it was therefore unusable for angular correlations. By this time the ruthenium nitroso had decomposed, probably to a complex ruthenium salt, so another plating could not be attempted.

The solution containing the $^{106}Ru$ was then evaporated in the bottom of a hole 6.35 mm deep by 2.36 mm in diameter drilled into a lucite rod. A small piece of cotton was placed in the bottom of the hole before the evaporation was started. The final source strength was approximately 0.5 mc and its dimensions were approximately 2.16 x 3.18 mm.

The table and electronics were set up as previously described. The procedure used in taking each data point and analyzing it is as follows:

1. The moveable detector is set at some angle with respect to the fixed detector. Then the equipment is allowed to count for twenty-four hours. This counting time was necessary to collect the necessary statistics to give counting errors on the order of five percent.
2. The results are printed out by the multichannel analyzer in the form of a single peak spectrum on top of a horizontal smooth background. See Figure 7.
3. The data point is analyzed by first summing the counts in each channel under the peak; denote this sum by N; then an equal number of background channels are summed; denoted by $N_A$. The number of true coincidences, $N_t$, is

$$N_t = N - N_A$$

The statistical error associated with $N_t$ is $\pm\sqrt{N+N_A}$

The above procedure was followed for thirty consecutive days. The moveable detector was moved alternately from one side of the $180^{\circ}$ line to the other side. Thus the correlation curve was swept out several times; and therefore, systematic errors which might tend to skew the curve should have been averaged out.

## CHAPTER III

## ANALYSIS AND CONCLUSIONS

After all the data were collected each data point was corrected for source decay with program FRED as given in Appendix A. The corrected data were then fitted by the method of least squares with program CORY as given in Appendix B to the function

$$R(\theta) = A_0 + A_2 P_2(\cos\theta + \delta) + A_4 P_4(\cos\theta + \delta). \qquad (3.1)$$

The unnormalized correlation coefficients $A_0$, $A_2$, and $A_4$ were obtained from this curve fitting. The program also fitted for $\delta$ as a counter check on the $^{22}Na$ correlation, where $\delta$ is the difference between the travel-dial zero and the actual $180^{\circ}$ position of the detectors. The results are

$$R(\theta) = 1342. + 254.4\ P_2(\cos\theta') + 1073.0\ P_4(\cos\theta'), \qquad (3.2)$$

and by normalizing $A_0$ to 1.0

$$W(\theta) = \frac{R(\theta)}{A_0} = 1 + 0.1895\ P_2\ (\cos\theta') + 0.7995\ P_4(\cos\theta'). \qquad (3.3)$$

$\delta$ is equal to 0.029 radius. $\theta'$ is equal to $\theta+\delta$.

These results have not been corrected for finite geometries. Figure 8 shows the half-life corrected data along with the computer fit.

Rose[11] has developed a method for calculating the geometrical correction factors for the NaI detectors previously used in angular correlation work. Figure 9 defines the dimensions and angles used in the derivation.

When the detectors for two radiations subtend finite solid angles $\Omega_1$ and $\Omega_2$, it is advisable to modify the theoretical correlation function and compare this attenuated correlation function with the measured one. The detectors are assumed to be crystals cut in the form of right circular cylinders with the base oriented towards the source. The source, at the origin, is on the intersection of the axes of the cylinders. In this case the form of the correlation function is unchanged and each coefficient $A_j$ becomes multiplied by an attenuation factor $Q_j$.

To take into account the absorption of the radiation in each detector, the following notation is introduced. The distance from the source to the front face of each detector is h, the thickness is t and r is the radius of each detector. The absorption in the detector is proportional to $(1-e^{-\tau x(\beta)})$ where $\tau$ is the absorption coefficient and $x(\beta)$ is the distance traversed by the radiation incident on the detector at an angle $\beta$ with respect to the axis. Then the measured correlation function would be

$$\overline{W(\Theta)} = \frac{\int d\Omega_1 d\Omega_2 W(\Theta') \ (1-e^{-\tau x_1}) \ (1-e^{-\tau x_2})}{\int d\Omega_1 d\Omega_2 (1-e^{-\tau x_1})(1-3^{-\tau x_2})} \qquad (3.4)$$

where the subscripts on the x's refer to the two detectors, $d\Omega_1$ and $d\Omega_2$ are the solid angle elements for each radiation, and $\Theta'$ is the angle between the propagation vectors of the $\gamma$-rays, while $\Theta$ is the angle between the cylinder axes.

From this the required integrals are of the form

$$I_j = \int d\Omega_1, \ d\Omega_2 \ P_j(\cos\Theta') \ (1-e^{-\tau x_1})(1-e^{-\tau x_2}), \qquad (3.5)$$

and from Figure 9 it is easily seen that

$$x(\beta) = t \sec\beta \text{ for } 0 \leq \beta \ \tan^{-1}\left[\frac{\tau}{(h+t)}\right] = \beta' \qquad (3.6)$$

$$x(\beta) = r \ c\mathrm{Sec}\beta - h \ \sec\beta \text{ for } \beta' \leq \beta \leq \tan^{-1}\left(\frac{r}{h}\right) = \gamma, \qquad (3.7)$$

where $\gamma$ is the half angle subtended by the front face of the detector. After using the addition theorem for spherical harmonics, the integration over $\phi_1$, the azimuth of direction of radiation 1, can be carried out since $x_1$ is independent of $\phi_1$. Applying the addition theorem once more to the spherical triangle formed by the axes of the two detectors and the direction of radiation 2 gives

$$P_j(\cos\Theta) = (P_j(\cos\Theta_2))(P_j(\cos\Theta_1')) + \ldots \qquad (3.8)$$

where azimuthal dependent terms have not been written out. On integration over $\phi_2$, for which the azimuthal dependent terms do not contribute, it is seen that

$$I_j = 4\Pi^2 P_j(\cos\Theta) J_j(1) J_j(2), \tag{3.9}$$

where $J_j$ is given by

$$J_j = \int_0^{\gamma} P_j(\cos\beta)\ (1-e^{-\tau x(\beta)}) \sin\beta d\beta. \tag{3.10}$$

The attenuation factor then is

$$Q_1 = \frac{J_j(1)}{J_0(1)} \cdot \frac{J_j(2)}{J_0(2)}\ . \tag{3.11}$$

Program FUBAR, Appendix C, was written to evaluate the integral in Equation 3.9. This integral must be evaluated for each j value (0,2, and 4) for each detector, or a total of six integrations. Figure 10 shows how $Q_2$ and $Q_4$ vary when the radius of one detector is varied. A similar result would be obtained if h for one detector was varied. This derivation assumed that the radii of the two detectors were the same; however, in Equation 3.11 it is seen that the correction factors split into two factors, one for each detector. Thus, two identical detectors are not necessary. The detectors used in this experiment were not identical. The fixed detector has a radius of 1.60 cm and the movable detector has a radius of 1.69 cm. Both detectors have drifted depths of 5 mm.

The correction factors calculated with program FUBAR for this experiment are

$Q_2 = 0.970$ and $Q_4 = 0.904$

This experiment's geometrically corrected correlation coefficients are compared in Table I with previously reported values.

TABLE I

| $A_2$ | $A_4$ | Reference |
|---|---|---|
| $0.3456 \pm 0.0079$ | $1.109 \pm 0.012$ | Klema |
| 0.314 | 1.058 | Ortabasi |
| $0.332 \pm 0.005$ | $1.060 \pm 0.008$ | Koch |
| 0.3571 | 1.143 | Theoretical[a] |
| $0.195 \pm 0.019$ | $0.887 \pm 0.088$ | This Work |

Correlation Coefficients for $^{106}Pd$

The results of this experiment do not give agreement, within the quoted errors, with the previously reported results for the 624-513 KeV cascade. Klema[7] reported that other correlations, besides the 624-513 KeV correlation, were present in $^{106}Pd$. Specifically, his results were corrected for the 1045-513 KeV cascade. However, calculations indicate that this competing cascade would change the measured values of the correlation coefficients by approximately one percent. This calculation assumed a flat Compton distribution from the 1045 KeV transition.

Koch[9] has reported a 612-513 KeV correlation. If this correlation exists, it could explain part of the discrepancy. From Figure 1, the decay scheme of $^{106}Pd$,[12] one can see that if the 1.125 KeV level is populated it should have a measurable effect on the 624-513 KeV correlation. Figure 11 shows a $^{106}Pd$ spectrum taken by one of the detectors used in this experiment. The 511 and 662 KeV $\gamma$-rays from $^{22}Na$ and $^{137}Cs$ respectively were used for energy calibration of the system. The calibration equation for this graph is $E = 0.315 \frac{KeV}{channel}$ (channel # - 257) + 511 KeV. The 612 KeV peak was not observed. The resolution of this detector at this energy is 4.5 KeV. Therefore, if the 1.125 KeV level is populated, then it would have easily been resolved. The conclusion from this work is that the 1.125 KeV level is not populated and therefore can have no effect on the correlation.

As stated previously, it had been planned to plate $^{106}Ru$ onto a copper foil to make a source. To do this, the $RuCl_3$ had been converted to ruthenium nitroso, which decomposed in a few hours. Thus the present chemical state of the $^{106}Ru$ is not known. When the $^{106}Ru$ was dried it is probable that a polycrystaline sample resulted.

The effect of a randomly oriented perturbation does not change the mathematical form of the angular correlation function. It results only in an attenuation of the coefficients of the $P_j(\cos\theta)$.[13] In other words, the effect of the perturbation is to multiply the $P_j(\cos\theta)$ by an attenuation factor $G_{jj}(t)$.

Thus, if the correlation is perturbed, it can be written in the form

$$W(\theta) = \Sigma A_j G_{jj}(t) P_j(\cos\theta) \qquad (3.12)$$

Steffen and Frauenfelder[13] have derived equations for calculating the $G_{jj}(t)$ for axially symetric quadrupole interactions in polycrystaline sources. However, the axially symetric electrostatic field gradient $V_{zz}$ must be known. Steffen[13] gives a graph for I = 2 from which rough values for $G_{jj}(\infty)$ should be obtainable. This graph is for time integrated $G_{jj}(t)$, which is the case for this experiment since the lifetime of the intermediate state in $^{106}Pd$ is twelve picoseconds and the resolving time is approximately twenty nanoseconds. If $G_{44}(\infty)$ is determined by forming the ratio of the experimental $A_4$ to the reported values of $A_4$, then $G_{22}(\infty)$ can be estimated from the graph given by Steffen. The average of the three reported values of $A_4$ given in Table 1 is 1.076. The $G_{44}(\infty)$ calculated by this method is 0.82. From the graph using this value for $G_{44}$, $G_{22}$ is found to be 0.68. From this the perturbation corrected correlation coefficients are

$$A_2 = 0.29 \text{ and } A_4 = 1.10.$$

This approach gives a possible explanation of the low values for the experimentally determined correlation coefficients of this work. Very little can be said about $A_2$ and $A_4$ determined by this method, other than that if an axially symetric

quadrupole iteraction is present in the sample then the perturbation attenuation factors should be approximately:

$$G_{22} = 0.68 \text{ and } G_{44} = 0.82.$$

It is reasonable to assume that this type perturbation may exist in the sample; otherwise, $A_2$ calculated by this method would most likely have been drastically different from the reported values. Further work should be done to check these results. To establish if the perturbation is actually present, the source could be re-liquefied. This should reduce the perturbation effects.

In summary, this work has shown

1. The previously reported $\gamma$-ray transition at 612 KeV is not present in the decay of 30 second $^{106}$Rh. The relative transition strength as compared to the 624 KeV transition is less than 1 to 50 instead of the 1 to 9 value previously reported.
2. The $^{106}$Pd 624-513 KeV correlation as measured in a complex chemical state appears to be perturbed. Consistent results for the correlation coefficients are obtained if a quadrupole perturbation is included as a correction factor.
3. Geometrical correction factors for Ge(Li) planar detectors may be calculated using a simple geometrical model for the detectors. This is in agreement with the work reported in the literature[14] and work to be published.[15]

# APPENDIX A

PROGRAM FRED

```
1  FORMAT(2F10.0)
10 FORMAT(14)
   DIMENSION EXI(100),TI(100),XI(50),CORI(100),ERCOR(100)
   READ 10,N
   DO 6 J=1,N
   TI(J)=J
6  READ 1,XI(J), EXI(J)
   DO 20 J=1,N
   CORI(J)=EXI(J)*EXPF(0.693*TI(J)/365.0)
   ERCOR(J)=SQRTF(4550.0+CORI(J))
   PUNCH 40, XI(J), CORI(J)
20 PRINT 30, CORI(J), EXI(J), ERCOR(J)
30 FORMAT (/3F20.3)
40 FORMAT (2E10.4)
   STOP
   END
```

# APPENDIX B

PROGRAM CORY

```
C       LEAST SQUARES CURVE FITTING -- METHOD OF DIFFERENTIAL
                                                        CORRECTION
C       NOBS = THE NUMBER OF (X,Y) PAIRS
C       NPAR = THE NUMBER OF PARAMETERS IN THE EQUATION
C       P(I) = THE ITH PARAMETER
C       RMS = ROOT MEAN SQUARE ERROR
C       A(I,J) = MATRIX FOR SIMULTANEOUS EQUATIONS
C       YC = THE CALCULATED VALUE OF THE FUNCTION AT X(K)
C       RES = RESIDUAL
C       T = TEMPORARY STORAGE
C       PF(I) = THE VALUE OF THE PARTIAL WITH RESPECT TO THE
                                            ITH PARAMETER AT X(K)
C       ITER = ITERATION NUMBER
C       PCE = PERCENTAGE ERROR
C       STATEMENT 9999 STARTS THE SUBROUTINE FOR CALCULATION
                    OF THE PARTIALS AND THE FUNCTION AT X(K)
        DIMENSION A(10,11), X(100), Y(100), P(10), PF(10), W(100)
        CONTROL 971
    1   READ 50, NOBS, NPAR, IWT
   50   FORMAT (313)
C       READ PARAMETERS
        DO 1000 I = 1, NPAR
 1000   READ 51, P(I)
   51   FORMAT (2E10.0)
```

```
C       READ (X,Y) PAIRS
        DO 2 I=1, NOBS
    2   READ 51, X(I), Y(I)
C       IWT=1, 2, OR 3 FOR W=1, W=1/ABSF(Y), W=1/Y**2.
        GO TO (60, 61, 62), IWT
   60   DO 70 I=1, NOBS
   70   W(I)=1.
        GO TO 2000
   61   DO 71 I=1, NOBS
   71   W(I)=1./ABSF(Y(I))
        GO TO 2000
   62   DO 72 I=1, NOBS
   72   W(I)=1./Y(I)**2
 2000   RMS=0
        OBS = NOBS
        N1 = NPAR + 1
        ITER = 0.
        FACTR = 1.0
    3   RMSQ = RMS
        RMS = 0
C       CONSTRUCT MATRIX
        DO 4 I = 1, NPAR
        DO 4 J = I, N1
    4   A(I,J) = 0.
        DO5K=1,NOBS
        M = 1
```

```
      GO TO 9999
 9998 RES = Y(K) - YC
      RMS = RES*RES + RMS
      DO 5 I = 1, NPAR
      T=PF(I)*W(K)
      A(I,N1) = A(I,N1) + RES*T
      DO 5 J=I, NPAR
    5 A (I,J) = A(I,J) + PF(J)*T
      DO 15I=I, NPAR
      DO 15J=I,NPAR
   15 A (J,I) = A(I,J)
      RMS = (RMS/OBS)**.5
C     SIMULTANEOUS EQUATION SOLUTION
      DO 6 K = 1, NPAR
      T = 1./A(K,K)
      KK = K + 1
      DO 7 L = KK, N1
    7 A(K,L) = A(K,L)*T
      DO 6 I = 1, NPAR
      IF (I-K) 8, 6, 8
    8 T = -A(I,K)
      DO 9 J = KK, N1
    9 A(I,J) = A(I,J) + T*A(K,J)
    6 CONTINUE
C     CORRECT PARAMETERS
      PRINT 56
```

```
   56 FORMAT (17X, 1HP, 16X, 7HDELTA P)
      IF (SENSE SWITCH 2) 20, 21
   20 READ 51, FACTR
   21 DO 10 I=1, NPAR
      T = A(I,N1)*FACTR
      P(I) = P(I) + T
   10 PRINT 52, I, P(I), T
   52 FORMAT (I5, 2E 19.7)
      ITER = ITER + 1
      PRINT 53, RMS, ITER
   53 FORMAT(/5X,5HRMS =,E15.8, 5X, 10HITERATION=, 13,////)
      IF (SENSE SWITCH 1) 11, 14
C     TEST RELATIVE CHANGE IN RMS AGAINST TOLERANCE
   14 IF(ABS((RMS-RMSQ)/RMS)-1.E-6)11,11,3
   11 CONTROL 971
C     BACK SOLUTIONS
      PRINT 54
   54 FORMAT (8X,1HX,16X,1HY,14X,2HYC,13X,4HDIFF,10X,8HP.C.
                                                        ERR)
      DO 12 K = 1, NOBS
      M = 2
      GO TO 9999
 9997 RMS = YC-Y(K)
      PCE = 100.*RMS/Y(K)
   12 PRINT 55, X(K), Y(K), YC, RMS, PCE
   55 FORMAT (5E16.8)
```

```
      CONTROL 971
      IF (SENSE SWITCH 1) 3,1
C     INSERT ROUTINE FOR CALCULATION OF PARTIALS, PF( ), AND
                                          FUNCTION, YC, AT X(K)
C     FIRST STATEMENT MUST BE NUMBERED 9999
 9999 TEMP = X(K) + P(4)
      TEMP1 = COS(TEMP)
      TEMP2 = TEMP1**2
      TEMP3 = TEMP1**SIN(TEMP)
      PF(1) = (3.*TEMP2 - 1.)*.5
      PF(2) = (35.*TEMP2**2 - 30.*TEMP2 + 3.)/8.
      PF(3) = 1.
      PF(4) = -3.*P(1)*TEMP3 - P(2)*(TEMP2*TEMP3*17.5 - 7.5
                                                    *TEMP3)
      YC = P(1)*PF(1) + P(2)*PF(2) + P(3)
C     END OF ROUTINE
      GO TO (9998, 9997), M
      END
```

# APPENDIX C

```
                    PROGRAM FUBAR

C     *   PH61612   DR. TOM GRAY              FORTRAN
C      DECK 1 OF 3
C      N=NUMBER OF ITERATIONS
C      J IS THE NUMBER OF ITERATION FOR THE EDGE EFFECT
C      H1=DISTANCE FROM SOURCE TO MOVABLE DETECTOR
C      H2=DISTANCE FROM SOURCE TO FIXED DETECTOR
C      T1=THICKNESS OF MOVABLE DETECTOR
C      T2=THICKNESS OF FIXED DETECTOR
C      R1=RADIUS OF MOVABLE DETECTOR
C      R2=RADIUS OF FIXED DETECTOR
C      E1=ENERGY OF GAMMA RAY FOR MOVABLE DETECTOR
C      E2=ENERGY OF GAMMA RAY FOR FIXED DETECTOR
C      S1 AND S2 ARE BETHE-SALTPETER EQUATIONS
C      Z=ATOMIC NUMBER OF THE DETECTOR MATERIAL
C     *STATE E1 AND E2 IN KEV
       READ,N,H1,T1,R1,E1,J
       READ,H2,T2,R2,E2,Z
       READ,TAU1,TAU2
       IF(TAU1) 12,10,12
   10  S1=-0.18+0.28*.43429*LOG(E1*1000./(Z**2))
   11  S2=-0.18+0.28*.43429*L)G(E2*1000./(Z**2))
       TAU1=(40.*S1*((Z-0.3)**5)/SQRT(E1**7))*0.04418
       TAU2=(40.*S2*((Z-0.3)**5)/SQRT(E2**7))*0.04418
```

```
12 BFIX1=ATAN(R1/(H1+T1))
13 BFIX2=ATAN(R2/(H2+T2))
   SUM10=0
   SUM20=0
   SUM12=0
   SUM22=0
   SUM14=0
   SUM24=0
   M=N/2
   L=M-1
   DO 5 I=1,L
   AI=I
   AN=N
   B1=2.*AI*BFIX1/AN
   B2=2.*AI*BFIX2/AN
   P1=COS(B1)
   P2=COS(B2)
   PL1=SIN(B1)
   PL2=SIN(B2)
   X1=T1/P1
   X2=T2/P2
   V10=(1.-EXP(-TAU1*X1))*PL1
   V20=(1.-EXP(-TAU2*X2))*PL2
   V12=0.5*((3.* (P1)**2.)-1.)*V10
   V22=0.5*((3.*(P2)**2.)-1.)*V20
   V14=0.125*(35.*((P1)**4.)-30.*((P1)**2.)+3.)*V10
```

```
      V24=0.125*(35.*((P2)**4.)-30.*((P2)**2.)+3.)*V20
      SUM10=SUM10+V10
      SUM20=SUM20+V20
      SUM12=SUM12+V12
      SUM22=SUM22+V22
      SUM14=SUM14+V14
      SUM24=SUM24+V24
    5   CONTINUE
C     *GAMMA=G
      G1=ATAN(R1/H1)
      G2=ATAN(R2/H2)
      EDG10=0
      EDG20=0
      EDG12=0
      EDG22=0
      EDG14=0
      EDG24=0
      L=J-1
      DO 6 I=1,L
      AI=I
      AJ=2*J
      B1=BFIX1+(2.*AI)*(G1-BFIX1)/AJ
      B2=BFIX2+(2.*AI)*(G2-BFIX2)/AJ
      P1=COS(B1)
      P2=COS(B2)
      PL1=SIN(B1)
```

```
      PL2=SIN(B2)
      V1=(R1/PL1)-H1/P1
      V2=(R2/PL2)-H2/P2
      W10=(1.-EXP(-TAU1*V1))*PL1
      W20=(1.-EXP(-TAU2*V2))*PL2
      W12=0.5*(3.*((P1)**2.)-1.)*W10
      W22=0.5*(3.*((P2)**2.)-1.)*W20
      W14=.125*(35.*((P1)**4.)-30.*((P1)**2)+3.)*W10
      W24=.125*(35.*((P2)**4.)-30.*((P2)**2)+3.)*W20
      EDG10=EDG10+W10
      EDG20=EDG20+W20
      EDG12=EDG12+W12
      EDG22=EDG22+W22
      EDG14=EDG14+W14
      EDG24=EDG24+W24
6     CONTINUE
      TOT10=0
      TOT20=0
      TOT12=0
      TOT22=0
      TOT14=0
      TOT24=0
      L=M-1
      DO 7 I=1,L
      AI=I
      AN=N
```

```
      B1=(2.*AI+1.)*BFIX1/AN
      B2=(2.*AI+1.)*BFIX2/AN
      P1=COS(B1)
      P2=COS(B2)
      PL1=SIN(B1)
      PL2=SIN(B2)
      X1=T1/P1
      X2=T2/P2
      C10=(1.-EXP(-TAU1*X1))*PL1
      C20=(1.=EXP(-TAU2*X2))*PL2
      C12=.5*(3.*((P1)**2.)-1)*C10
      C22=.5*(3.*((P2)**2.)-1)*C20
      C14=.125*(35.*((P1)**4.)-30.*((P1)**2.)+3.)*C10
      C24=.125*(35.*((P2)**4.)-30.*((P2)**2.)+3.)*C20
      TOT10=TOT10+C10
      TOT20=TOT20+C20
      TOT12=TOT12+C12
      TOT22=TOT22+C22
      TOT14=TOT14+C14
      TOT24=TOT24+C24
7     CONTINUE
      PRINT 111, SUM10, SUM20, SUM12, SUM22, SUM14, SUM24
      PUNCH 111, SUM10, SUM20, SUM12, SUM22, SUM14, SUM24
      PRINT 111, EDG10, EDG20, EDG12, EDG22, EDG14, EDG24
      PUNCH 111, EDG10, EDG20, EDG12, EDG22, EDG14, EDG24
      PRINT 111, TOT10, TOT20, TOT12, TOT22, TOT14, TOT24
```

```
      PUNCH 111, TOT10, TOT20, TOT12, TOT22, TOT14, TOT24
  111 FORMAT(6E11.5/)
      STOP
      END
END OF COMPILATION
C     *   PH61612   DR. TOM GRAY          FORTRAN
C      DECK 2 OF 3
C     *GEOMETRICAL CORRECTION-ROSES METHOD
C      N=NUMBER OF ITERATIONS
C      J IS THE NUMBER OF ITERATION FOR THE EDGE EFFECT
C      H1=DISTANCE FROM SOURCE TO MOVABLE DETECTOR
C      H2=DISTANCE FROM SOURCE TO FIXED DETECTOR
C      T1=THICKNESS OF MOVABLE DETECTOR
C      T2=THICKNESS OF FIXED DETECTOR
C      R1=RADIUS OF MOVABLE DETECTOR
C      R2=RADIUS OF FIXED DETECTOR
C      E1=ENERGY OF GAMMA RAY FOR MOVABLE DETECTOR
C      E2=ENERGY OF GAMMA RAY FOR FIXED DETECTOR
C      S1 AND S2 ARE BETHE-SALTPETER EQUATIONS
C      Z=ATOMIC NUMBER OF THE DETECTOR MATERIAL
C     *STATE E1 AND E2 IN KEV
      READ,N,H1,T1,R1,E1,J
      READ,H2,T2,R2,E2,Z
      READ,TAU1,TAU2
      IF(TAU1) 12,10,12
   10 S1=-0.18+0.28*.43429*LOG(E1*1000./(Z**2))
```

```
11 S2=-0.18+0.28*.43429*LOG(E2*1000./(Z**2))
   TAU1=(40.*S1*((Z-0.3)**5)/SQRT(E1**7))*0.04418
   TAU2=(40.*S2*((Z-0.3)**5)/SQRT(E2**7))*0.04418
12 BFIX1=ATAN(R1/(H1+T1))
13 BFIX2=ATAN(R2/(H2+T2))
   PRINT 111,TAU1,TAU2
   ZZZZ=CON(951.1)
   M=N/2
   EDE10=0
   EDE20=0
   EDE12=0
   EDE22=0
   EDE14=0
   EDE24=0
   L=J-1
   DO 8 I=1,L
   AI=I
   G1=ATAN(R1/H1)
   G2=ATAN(R2/H2)
   AJ=2*J
   B1=BFIX1+(2.*AI+1.)*(G1-BFIX1)/AJ
   B2=BFIX2+(2.*AI+1.)*(G2-BFIX2)/AJ
   U1=(R1/SIN(B1))-H1/COS(B1)
   U2=(R2/SIN(B2))-H2/COS(B2)
   D10=(1.-EXP(-TAU1*U1))*SIN(B1)
   D20=(1.-EXP(-TAU2*U2))*SIN(B2)
```

```
      D12=.5*(3.*((COS(B1))**2.)-1.)*D10
      D22=.5*(3.*((COS(B2))**2.)-1.)*D20
      D14=.125*(35.*((COS(B1))**4.)-30.*((COS(B1))**2.)+3.)
     *D10
      D24=.125*(35.*((COS(B2))**4.)-30.*((COS(B2))**2.)+3.)
     *D20
      EDE10=EDE10+D10
      EDE20=EDE20+D20
      EDE12=EDE12+D12
      EDE22=EDE22+D22
      EDE14=EDE14+D14
      EDE24=EDE24+D24
    8 CONTINUE
      PUNCH 111, EDE10, EDE20, EDE12, EDE22, EDE14, EDE24
      PRINT 111, EDE10, EDE20, EDE12, EDE22, EDE14, EDE24
      AN=N
      B1=BFIX1/AN
      B2=BFIX2/AN
      X1=T1
      X2=T2
      E10=(1.-EXP(-TAU1*X1))*SIN(B1)
      E20=(1.-EXP(-TAU2*X2))*SIN(B2)
      E12=.5*(3.*((COS(B1))**2.)-1.)*E10
      E22=.5*(3.*((COS(B2))**2.)-1.)*E20
      E14=.125*(35.*((COS(B1))**4.)-30.*((COS(B1))**2.)+3.)
     *E10
      E24=.125*(35.*((COS(B2))**4.)-30.*((COS(B2))**2.)+3.)
     *E20
```

```
      PRINT 111, E10, E20, E12, E22, E14, E24
      PUNCH 111, E10, E20, E12, E22, E14, E24
      B1=BFIX1
      B2=BFIX2
      X1=T1/COS(B1)
      X2=T2/COS(B2)
      F10=(1.-EXP(-TAU1*X1))*SIN(B1)
      F20=(1.-EXP(-TAU2*X2))*SIN(B2)
      F12=.5*(3.*((COS(B1))**2.)-1.)*F10
      F22=.5*(3.*((COS(B2))**2.)-1.)*F20
      F14=.125*(35.*((COS(B1))**4.)-30.*((COS(B1))**2.)+3.)
                                                        *F10
      F24=.125*(35.*((COS(B2))**4.)-30.*((COS(B2))**2.)+3.)
                                                        *F20
      PUNCH 111, F10, F20, F12, F22, F14, F24
      PRINT 111, F10, F20, F12, F22, F14, F24
  111 FORMAT(6E11.5/)
      STOP
      END
END OF COMPILATION
C     *PH61612   DR. TOM GRAY              FORTRAN
C     *GEOMETRICAL CORRECTION-ROSES METHOD DECK 3 OF 3
      READ,N,H1,T1,R1,F1,J,TAU1
      READ,H2,T2,R2,E2,Z,TAU2
      IF(TAU1) 12,10,12
   10 S1=-0.18+0.28*.43429*LOG(E1*1000./(Z**2))
   11 S2=-0.18+0.28*.43429*LOG(E2*1000./(Z**2))
```

```
      TAU1=(40.*S1*((Z-0.3)**5)/SQRT(E1**7))*0.04418
      TAU2=(40.*S2*((Z-0.3)**5)/SQRT(E2**7))*0.04418
   12 BFIX1=ATAN(R1/(H1+T1))
   13 BFIX2=ATAN(R2/(H2+T2)
      M=N/2
      READ 111, SUM10, SUM20, SUM12, SUM22, SUM14, SUM24
      READ 111, EDG10, EDG20, EDG12, EDG22, EDG14, EDG24
      READ 111, TOT10, TOT20, TOT12, TOT22, TOT14, TOT24
      READ 111, EDE10, EDE20, EDE12, EDE22, EDE14, EDE24
      READ 111, E10, E20, E12, E22, E14, E24
      READ 111, F10, F20, F12, F22, F14, F24
      AN=N
      AJ=2*J
      G1=ATAN(R1/H1)
      G2=ATAN(R2/H2)
      B1=BFIX1+(G1-BFIX1)/AJ
      B2=BFIX2+(G2-BFIX2)/AJ
      X1=(R1/SIN(B1))-H1/COS(B1)
      X2=(R2/SIN(B2))-H2/COS(B2)
      A10=(1.-EXP(-TAU1*X1))*SIN(B1)
      A20=(1.-EXP(-TAU2*X2))*SIN(B2)
      A12=.5*(3.*((COS(B1))**2.)-1.)*A10
      A22=.5*(3.*((COS(B2))**2.)-1.)*A20
      A14=.125*(35.*((COS(B1))**4.)-30.*((COS(B1))**2.)+3.)
                                                        *A10
      A24=.125*(35.*((COS(B2))**4.)-30.*((COS(B2))**2.)+3.)
                                                        *A20
```

```
B1=G1-(G1-BFIX1)/AJ
B2=G2-(G2-BFIX2)/AJ
G10=(1.-EXP(-TAU1*X1))*SIN(B1)
G20=(1.-EXP(-TAU2*X2))*SIN(B2)
G12=.5*(3.*((COS(B1))**2.)-1.)*G10
G22=.5*(3.*((COS(B2))**2.)-1.)*G20
G14=.125*(35.*((COS(B1))**4.)-30.*((COS(B1))**2.)+3.)
                                                *G10
G24=.125*(35.*((COS(B2))**4.)-30.*((COS(B2))**2.)+3.)
                                                *G20
VA10=(1./3.)*(BFIX1/AN)*(2.*SUM10+4.*TOT10+F10+E10)
VA20=(1./3.)*(BFIX2/AN)*(2.*SUM20+4.*TOT20+E20+F20)
VA12=(1./3.)*(BFIX1/AN)*(2.*SUM12+4.*TOT12+E12+F12)
VA22=(1./3.)*(BFIX2/AN)*(2.*SUM22+4.*TOT22+E22+F22)
VA14=(1./3.)*(BFIX1/AN)*(2.*SUM14+4.*TOT14+E14+F14)
VA24=(1./3.)*(BFIX2/AN)*(2.*SUM24+4.*TOT24+E24+F24)
EA10=(1./3.)*((G1-BFIX1)/AJ)*(2.*EDG10+4.*EDE10+G10+A10)
EA20=(1./3.)*((G2-BFIX2)/AJ)*(2.*EDG20+4.*EDE20+G20+A20)
EA12=(1./3.)*((G1-BFIX1)/AJ)*(2.*EDG12+4.*EDE12+G12+A12)
EA22=(1./3.)*((G2-BFIX2)/AJ)*(2.*EDG22+4.*EDE22+G22+A22)
EA14=(1./3.)*((G1-BFIX1)/AJ)*(2.*EDG14+4.*EDE14+G14+A14)
EA24=(1./3.)*((G2-BFIX2)/AJ)*(2.*EDG24+4.*EDE24+G24+A24)
AJ10=VA10+EA10
AJ20=VA20+EA20
AJ12=VA12+EA12
AJ22=VA22+EA22
AJ14=VA14+EA14
```

```
      AJ24=VA24+EA24
      PRINT 111, AJ10, AJ20, AJ12, AJ22, AJ14, AJ24
      R1210=AJ12/AJ10
      R1410=AJ14/AJ10
      R2220=AJ22/AJ20
      R2420=AJ24/AJ20
      Q2=R1210*R2220
      Q4=R1410*R2420
      PRINT 111, R1210, R1410, R2220, R2420, Q2,Q4
  111 FORMAT(6E11.5/)
      STOP
      END
END OF COMPILATION
```

# APPENDIX D

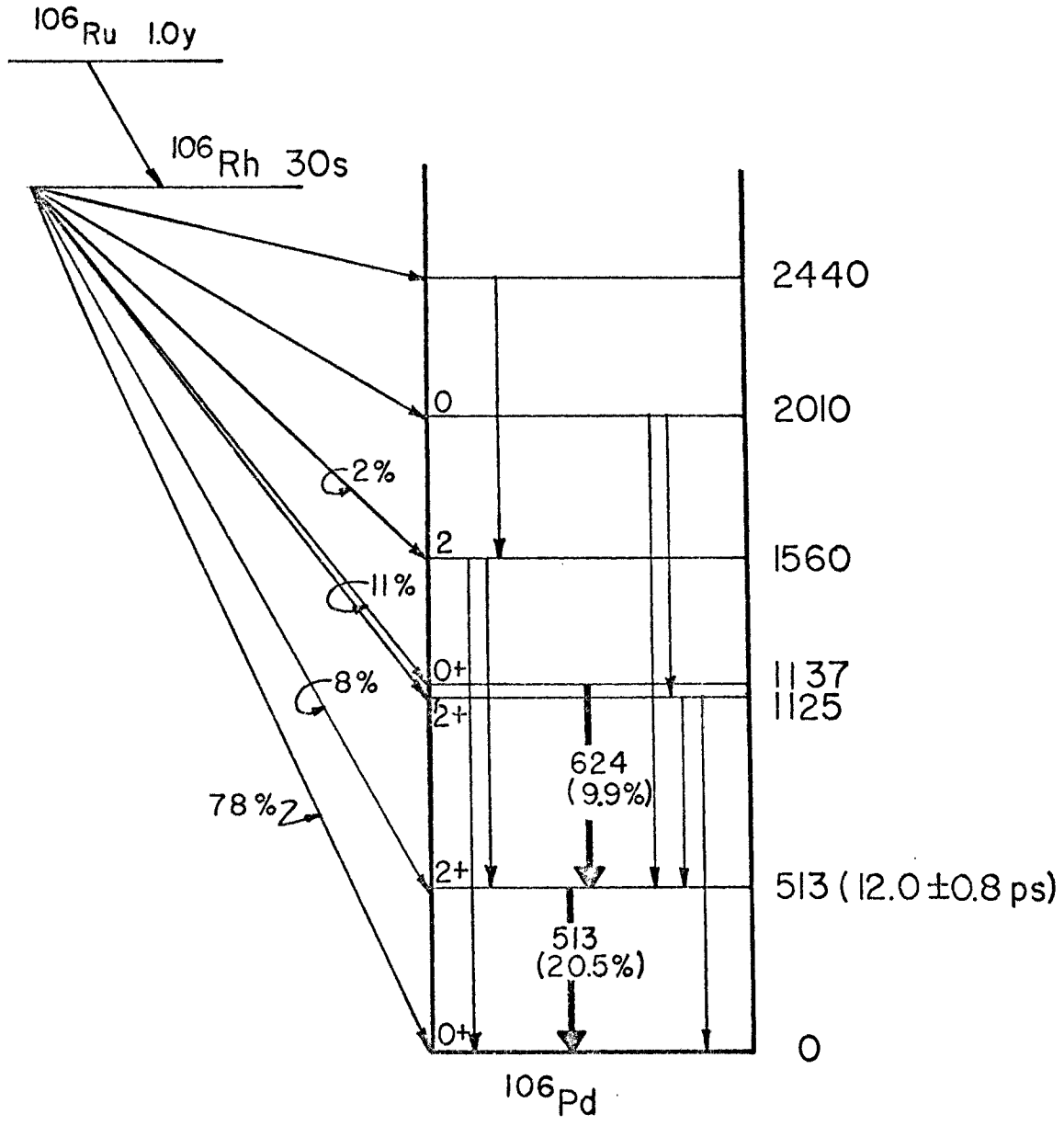


Figure 1 -- Decay Scheme of $^{106}Pd$

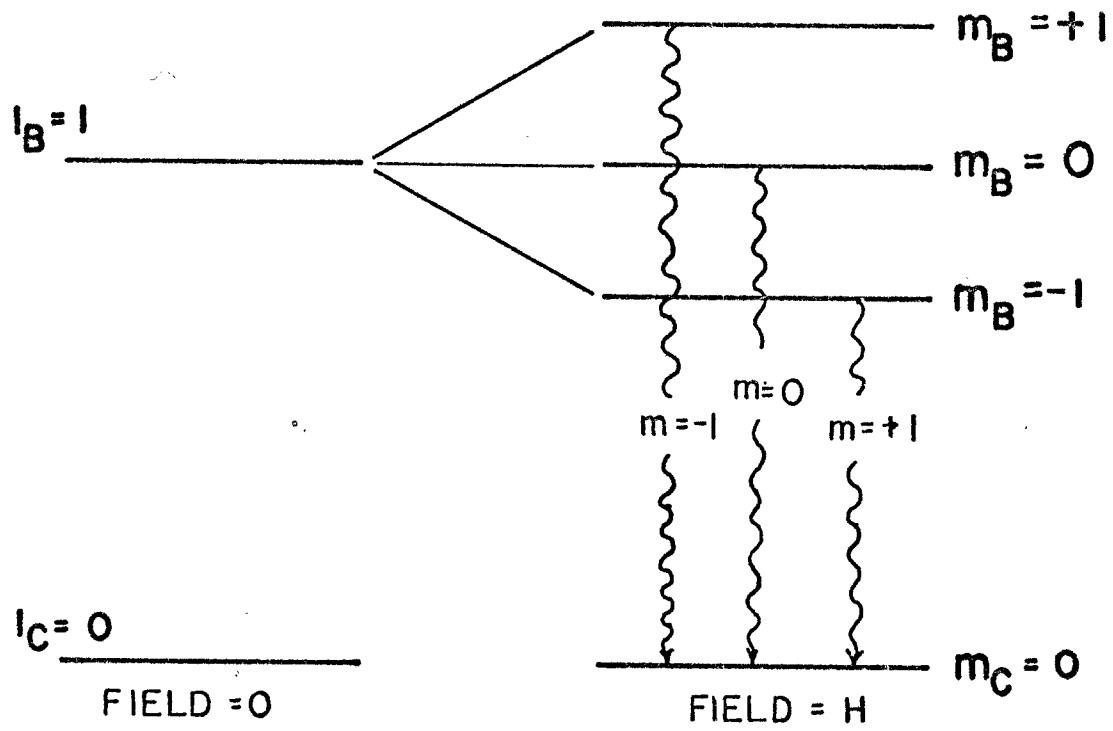


Figure 2. Magnetic Sublevels

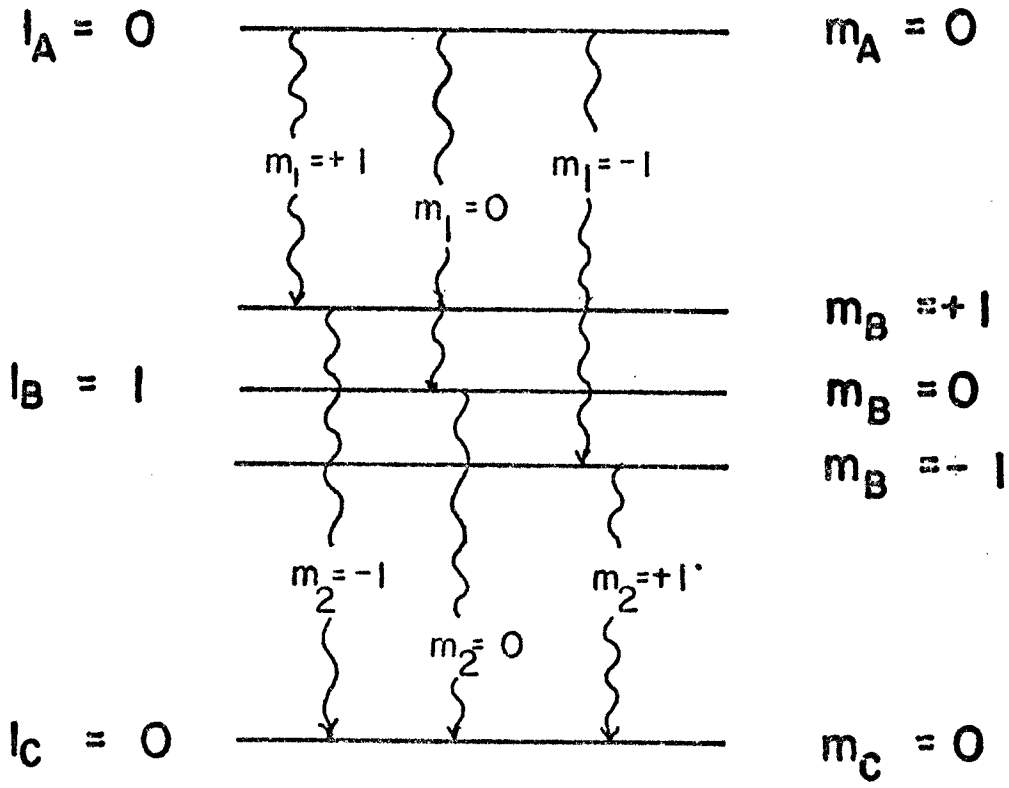


Figure 3 --γ-Ray Transitions Between Three Nuclear Levels

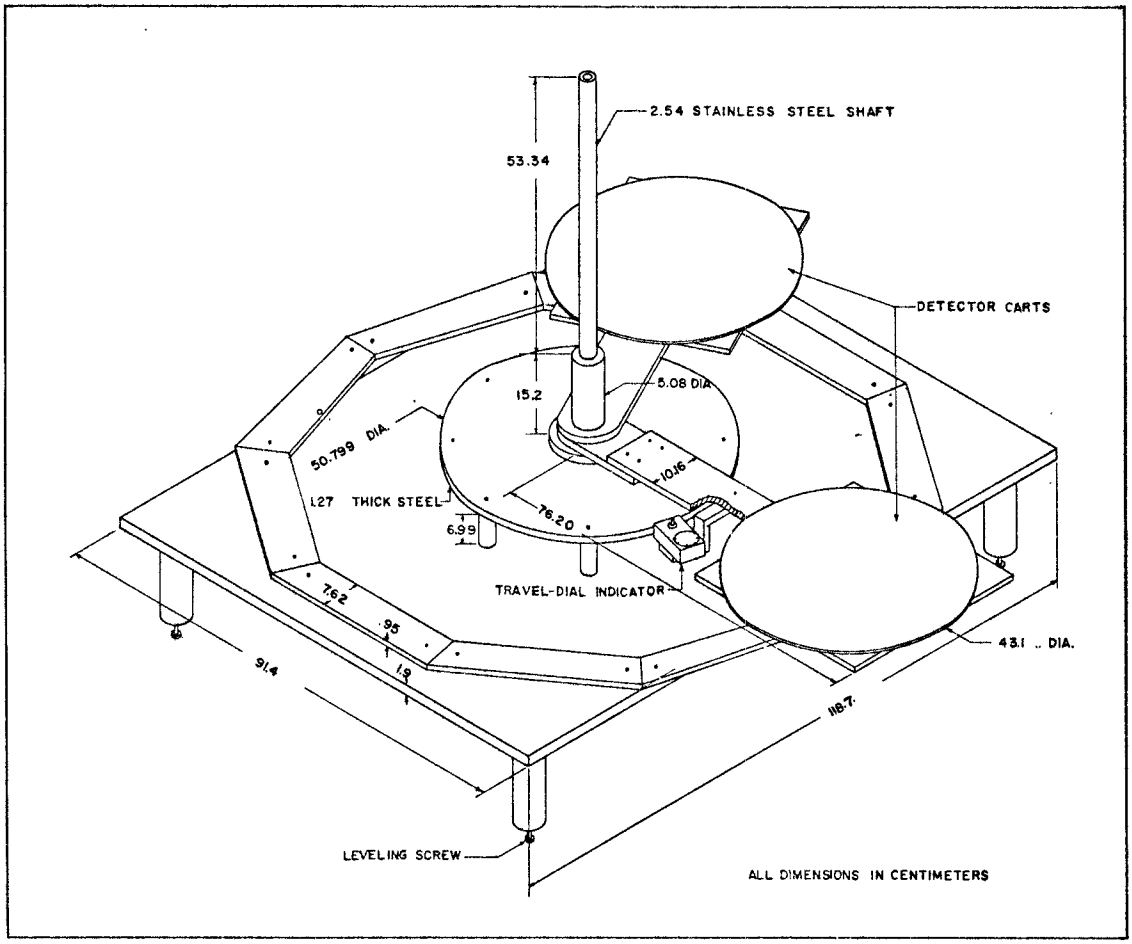


Figure 4 --Angular Correlation Table

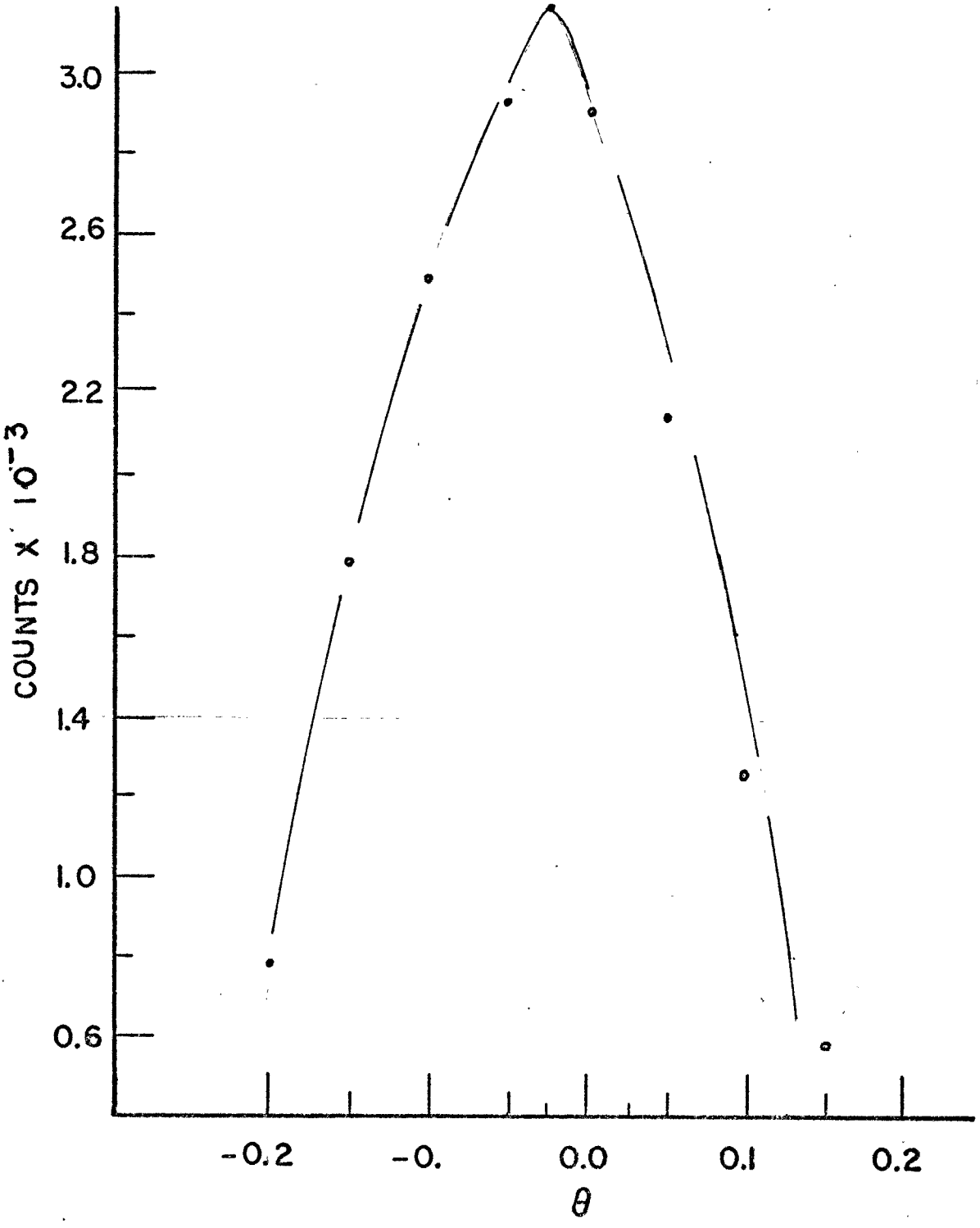


Figure 5 -- $^{22}Na$ Correlation

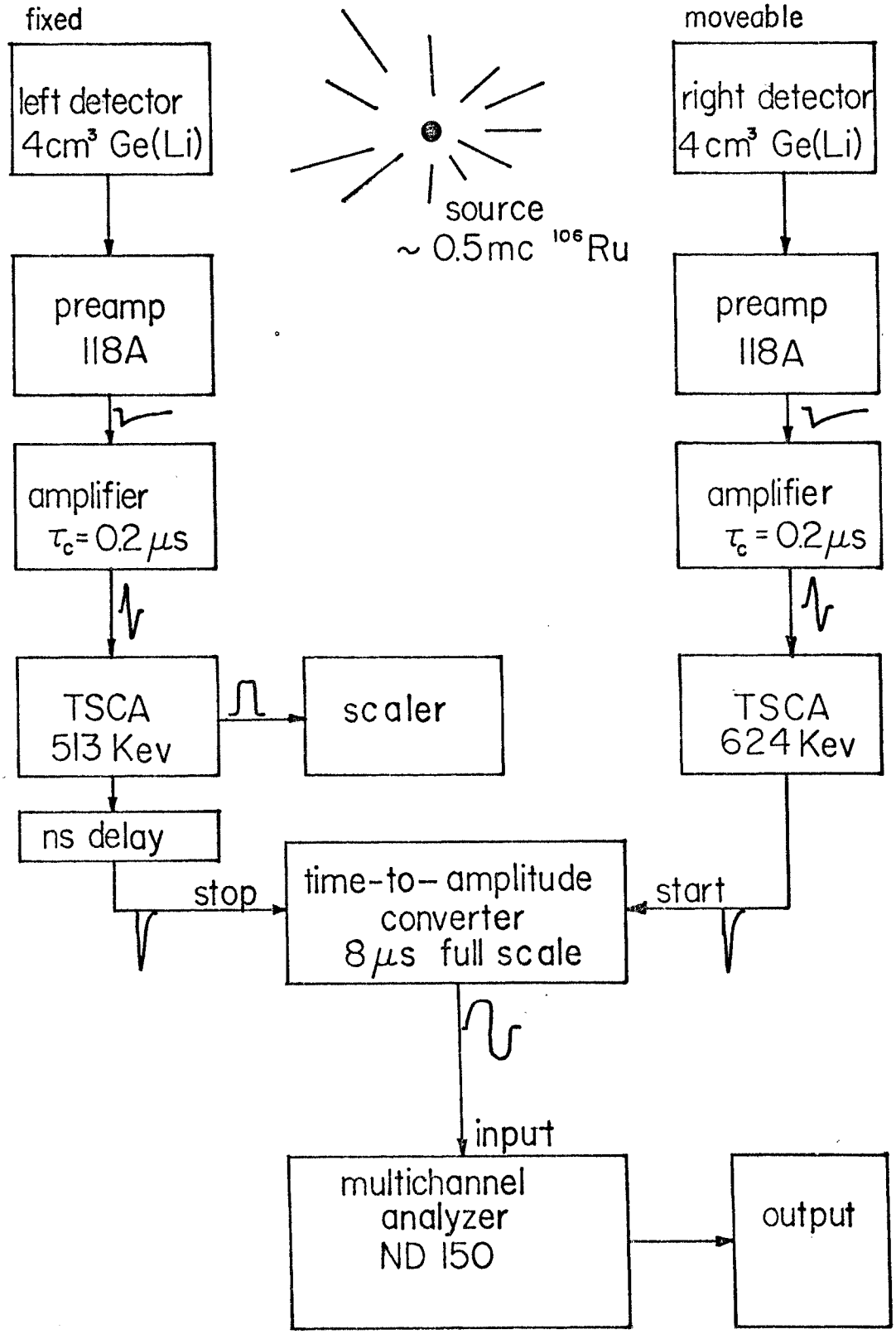


Figure 6--Block Diagram of Electronics

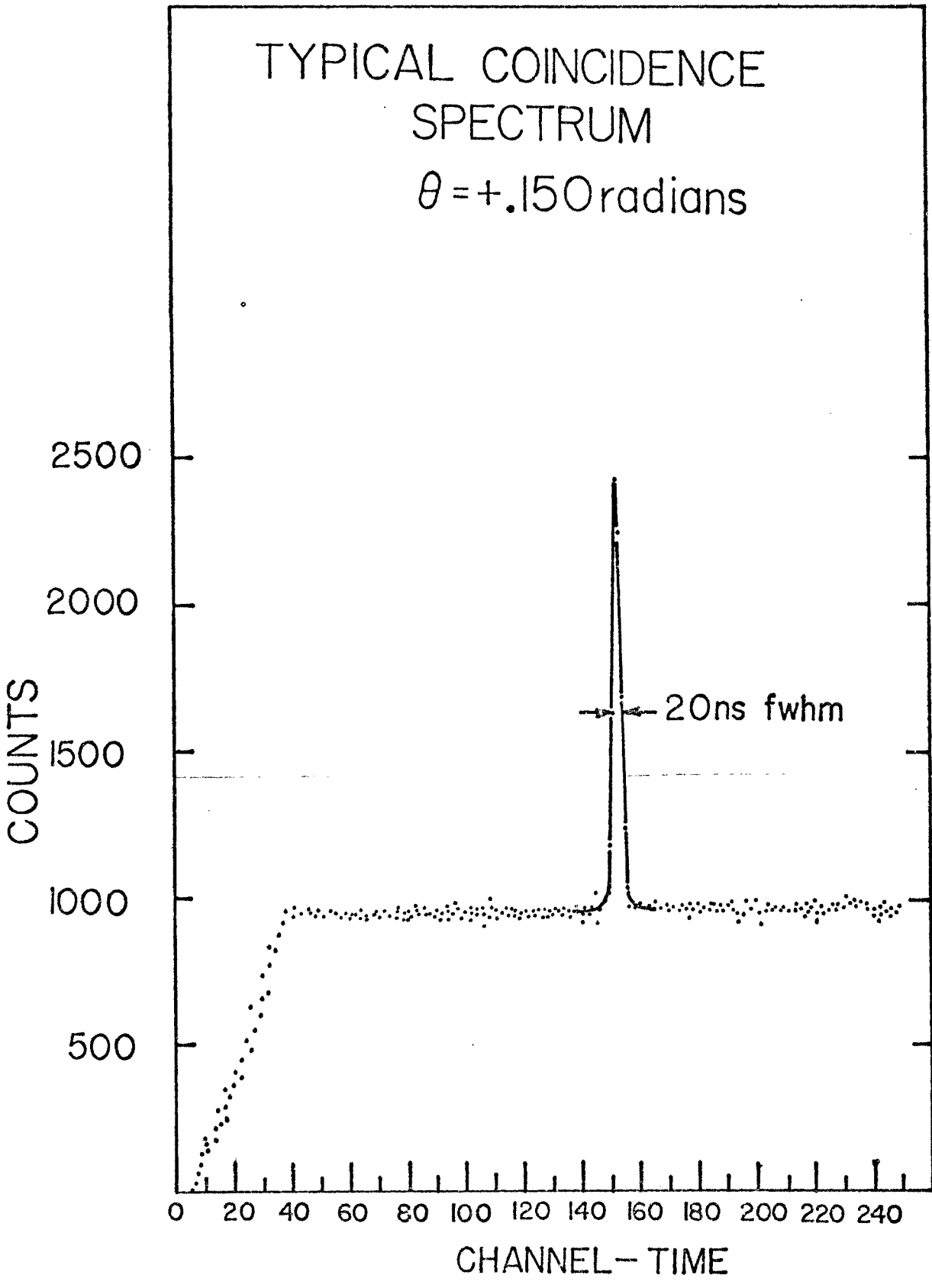


Figure 7- -Time Spectrum

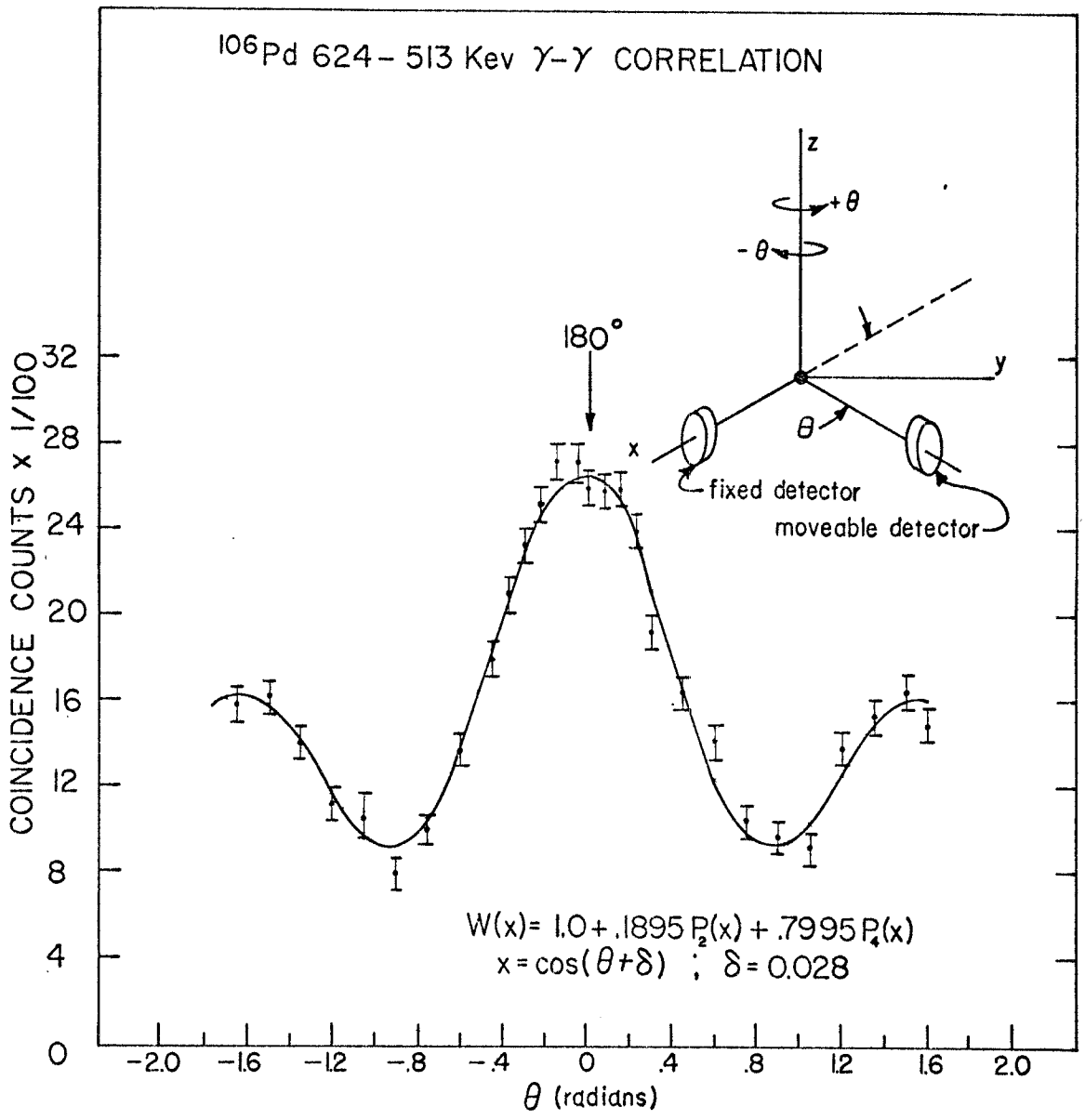


Figure 8 -- Half Life Corrected

Data and Least Squares Fit to the Data.

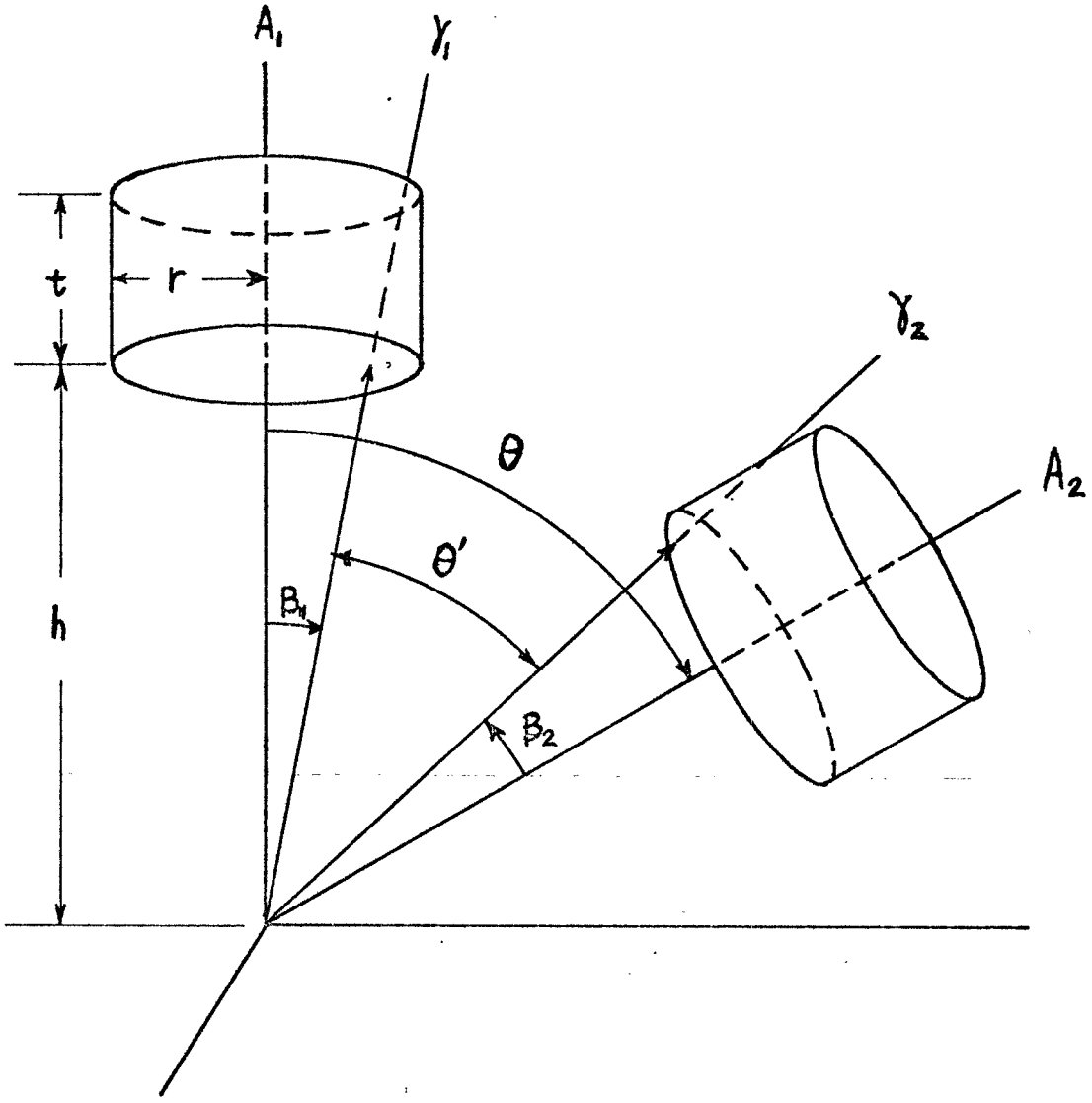


Figure 9--Geometry Used for Rose's Derivation

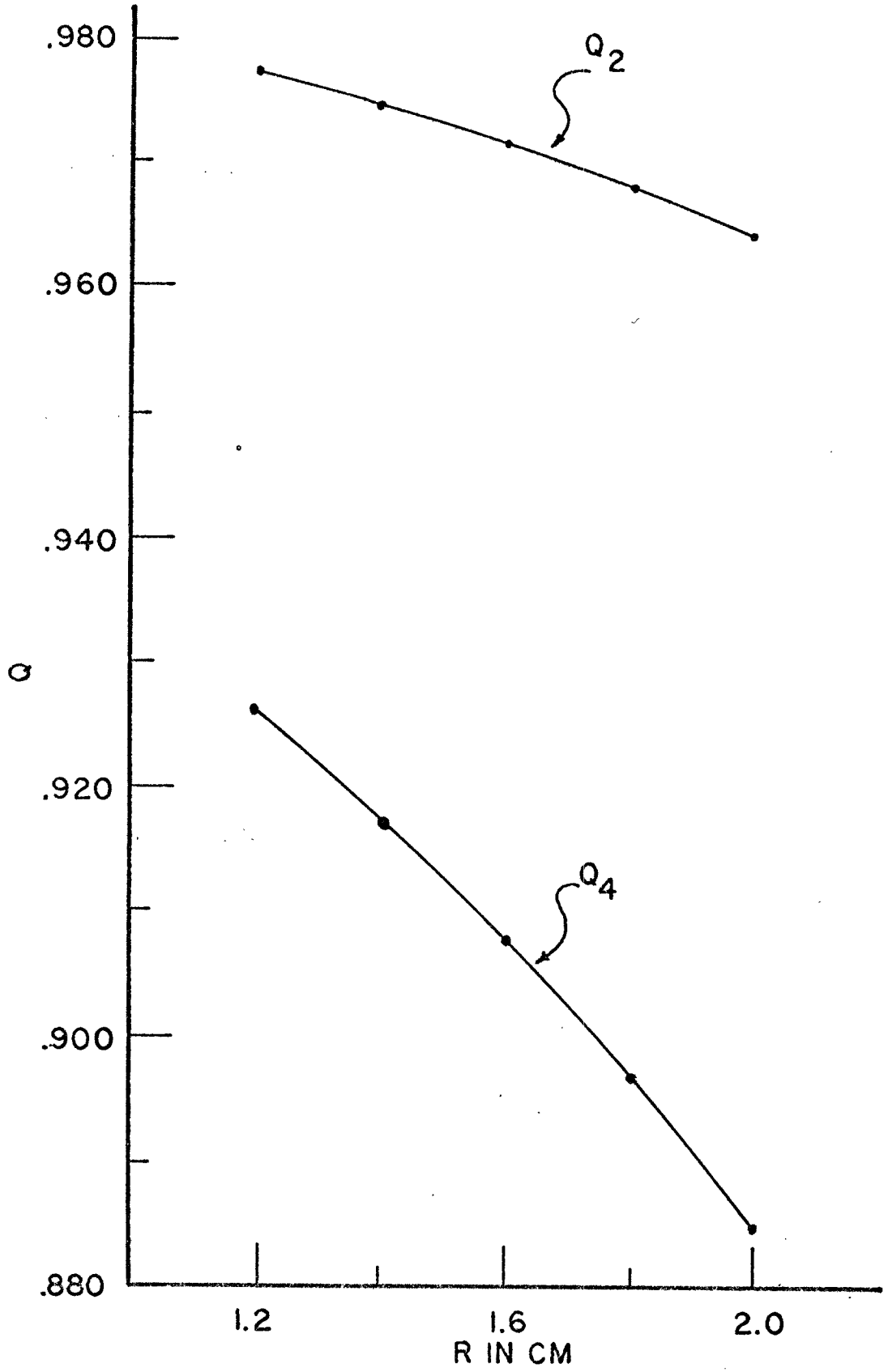


Figure 10__ Variation of

$Q_2$ and $Q_4$ With the Radius of One Detecto

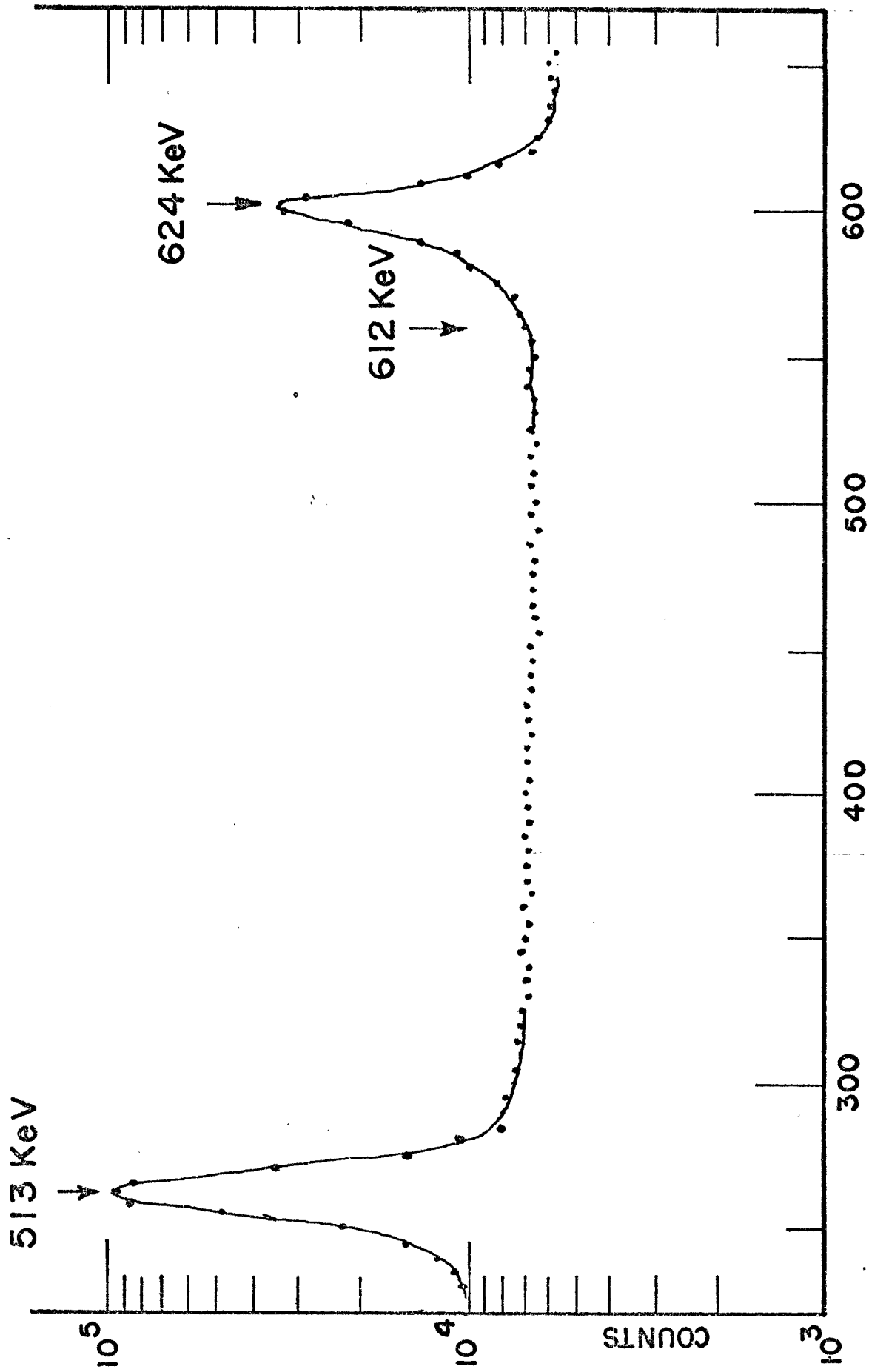


Figure 11-- Partial $^{106}$Pd Spectrum

FOOTNOTES


1. D. R. Hamilton, Phys. Rev. 58, 122 (1940).

2. S. P. Lloyd, Phys. Rev. 81, 307 (1951).

3. D. L. Falkoff and G. E. Uhlenbeck, Phys. Rev. 79, 323 (1950).

4. D. S. Ling and D. L. Falkoff, Phys. Rev. 76. 1639 (1949).

5. G. Racah, Phys. Rev. 82, 309 (1951).

6. M. E. Rose and L. C. Biedenharn, Rev. Mod. Phys. 25, 729 (1953).

7. E. D. Klema and F. K. McGowen, Phys. Rev. 92, 1469-1472 (1955).

8. U. Ortabasi and H. J. Korner, Nucl. Phys. 70, 28-32 (1965).

9. J. Koch, F. Munnich, and U. Schotzig, Nucl. Phys. A103, 300-310 (1967).

10. R. D. Evans, The Atomic Nucleus (McGraw-Hill Book Co., N. Y., 1955) 234-248.

11. M. E. Rose, Phys. Rev. 91, 610-615 (1953).

12. Nuclear Data Group (ed.), Nuclear Data Sheets, Part 4, 820 (1965), (no vol. no.)

13. R. M. Steffen and H. Frauenfelder, "The Influence of Extranuclear Fields on Angular Correlations," Part 1 of Perturbed Angular Correlations, edited by E. Karlsson and Others, (North-Holland Publishing Co., Amsterdam, 1964), 13-21.

14. F. T. Avignone and G. D. Frey, Rev. Sci. Instr. 39, 1941-1943 (1968).

15. D. C. Camp, Private Communication, August, 1969.

FOOTNOTE FOR TABLE I

a. K. Siegbahn, editor, Beta- and Gamma-Ray Spectroscopy (North-Holland Publishing Co., Amsterdam, 1955), Chap. 19, 556.

# BIBLIOGRAPHY

## Articles


Avignone, F. T., and Frey, G. D., "Angular Correlation and Distribution Attenuation Coefficients for Planar and Coaxial Ge(Li) Detectors," Rev. Sci. Instr. 39, 1941-43 (1968).

Falkoff, D. L., and Uhlenbeck, G. E., "On the Directional Correlation of Successive Nuclear Radiations," Phys. Rev. 79, 323-33 (1950).

Hamilton, D. R., "On Directional Correlation of Successive Quanta," Phys. Rev. 58, 122-31 (1940).

Klema, E. D., and McGowen, F. K., "Gamma-Gamma Angular Correlation in $^{106}$Pd, Phys. Rev. 92, 1469-72 (1955).

Koch, J., Munnich, F., and Schotzig, U., "Messung Des E2/M1 Mischungsverhaltnisses Von $2^+$-$2^+$ Ubergangen in $^{82}$Kr, $^{106}$Pd, $^{122}$Te, $^{192}$Pt Und $^{198}$Hg," Nucl. Phys. A103, 300-10 (1967).

Ling, D. S., and Falkoff, D. L., "Interference Effects in Gamma-Gamma Angular Correlations," Phys. Rev. 76, 1639-48 (1949).

Lloyd, S. P., "Some General Angular Correlation Formulas," 307 (1951).

Nuclear Data Group (ed.) Nuclear Data Sheets, Part 4, 820 (1965), (no vol. no.)

Ortabasi, U., and Körner, H. J., "Measurement of the g-Factor of the First Excited State in $^{106}$Pd," Nucl. Phys. 70, 28-32 (1965).

Racah, G., "On the Directional Correlation of Successive Nuclear Radiations," Phys. Rev. 82, 309 (1951).

Rose, M. E., "The Analysis of Angular Correlation and Angular Distribution Data," Phys. Rev. 91, 610-15 (1953).

Rose, M. E., and Biedenharn, L. C., "Theory of Angular Correlation of Nuclear Radiation," Rev. Mod. Phys. 25, 729-77 (1953).

## Books

Evans, R. D., The Atomic Nucleus (McGraw-Hill Book Co., N. Y., 1955) 234-48.

Siegbahn, K., editor, Beta- and Gamma-Ray Spectroscopy (North-Holland Publishing Co., Amsterdam, 1955) 556.

Steffen, R. M., and Frauenfelder, H., "The Influence of Extranuclear Fields on Angular Correlations," Part 1 of Perturbed Angular Correlations, edited by E. Karlsson and Others (North-Holland Publishing Co., Amsterdam, 1964), 13-21.

## Unpublished Materials

Camp, D. C., Lawrence Radiation Laboratory, University of California, Private Communication, August 1969.